Synthesis of a Far-Red Photoactivatable Silicon-Containing Rhodamine for Super-Resolution Microscopy

*Jonathan B. Grimm, Teresa Klein, Benjamin G. Kopek, Gleb Shtengel, Harald F. Hess, Markus Sauer, and Luke D. Lavis**

Abstract: The rhodamine system is a flexible framework for building small-molecule fluorescent probes. Changing N-substitution patterns and replacing the xanthene oxygen with a dimethylsilicon moiety can shift the absorption and fluorescence emission maxima of rhodamine dyes to longer wavelengths. Acylation of the rhodamine nitrogen atoms forces the molecule to adopt a nonfluorescent lactone form, providing a convenient method to make fluorogenic compounds. Herein, we take advantage of all of these structural manipulations and describe a novel photoactivatable fluorophore based on a Si-containing analogue of Q-rhodamine. This probe is the first example of a "caged" Si-rhodamine, exhibits higher photon counts compared to established localization microscopy dyes, and is sufficiently red-shifted to allow multicolor imaging. The dye is a useful label for super-resolution imaging and constitutes a new scaffold for far-red fluorogenic molecules.

Fluorescence microscopy enables the visualization of molecules in biological samples and is a critical tool in cell biology. The resolution of conventional microscopy is limited by the diffraction of light. This is described by Abbe's Law, $d = \lambda/2NA$, where d is the resolution limit, λ is the wavelength of light, and NA is the numerical aperture of the microscope objective. A method to overcome the diffraction limit involves sequentially activating sparse subsets of fluorescent molecules, imaging them until they bleach, and localizing each molecule with high precision. This technique, called photoactivated localization microscopy (PALM) or direct stochastic optical reconstruction microscopy (*d*STORM), enables imaging of cellular components at the nm scale[1] and has been extended to three-dimensions using interferometric methods[2] and other strategies.[3]

The fulcrum of localization microscopy imaging is the photoactivatable label. To be useful, these fluorophores must meet several strict requirements: low background fluorescence in the dark state, high photon yields upon activation, and an attachment strategy for cellular structures. Three major types of photoactivatable fluorophores have emerged as viable labels for localization microscopy. The first class involves photoactivatable or photoconvertible fluorescent proteins, such as mEos2 and other variants.[4] The second class of localization microscopy label consists of single conventional dyes that can be made photoswitchable under reducing conditions,[5] either by direct reduction of the dye[6] or formation of thiol-dye or phosphine-dye adducts[7] (i.e., *d*STORM dyes). The third class of localization microscopy labels are "caged" fluorophores where a synthetic fluorophore is appended with a photolabile group that can be removed or modified by illumination with short wavelength light to elicit a large change in fluorescence.[3c, 8]

Caged fluorophores have particular advantages as labels for localization microscopy. They typically exhibit higher photon counts than fluorescent proteins, leading to better localization precision. Additionally, caged fluorophores are activated by a photochemical reaction that is defined by the chemical structure of the compound, allowing sparse, controlled turn-on of individual molecules.[3c, 8] This eliminates the need for harsh, dye-specific environmental conditions to elicit photoswitching, as required for *d*STORM dyes.[1d, 5b, 6b–d] Despite these advantages, caged fluorophores have not been utilized extensively in localization microscopy owing to their challenging syntheses and a limited color palette. Although a few red caged fluorophores have been developed,[8e, 9] only dyes with green or orange emission have demonstrated utility in PALM;[3c, 8] these dyes have not been used in multicolor localization microscopy experiments. Thus, facile chemistry towards caged fluorophores with red absorption and emission would expand the current collection of localization microscopy labels and enable multicolor super-resolution imaging experiments using these versatile dyes.

We previously developed an efficient synthetic route to a derivative of Q-rhodamine (Rh$_Q$; Q for tetrahydroquinoline) bearing nitroveratryl oxycarbonyl (NVOC) caging groups (**1**, Scheme 1).[8c] To allow facile installation of the photolabile groups we used a reduced, *leuco*-rhodamine as a synthetic intermediate (Scheme 1). This caged Rh$_Q$ exhibits excellent photoactivation parameters and photon yield, enabling the first localization microscopy imaging of DNA in a cellular context.[8c] Nonetheless, the emission maximum of Rh$_Q$ is still green, complicating multicolor imaging with other photoactivatable labels. To overcome this problem, we

[*] J. B. Grimm, Dr. B. G. Kopek, Dr. G. Shtengel, Dr. H. F. Hess,
    Dr. L. D. Lavis
    Janelia Research Campus
    Howard Hughes Medical Institute
    19700 Helix Drive, Ashburn, VA 20147 (USA)
    E-mail: lavisl@janelia.hhmi.org

    Dr. T. Klein, Prof. Dr. M. Sauer
    Department of Biotechnology and Biophysics
    Julius Maximilian University Wuerzburg
    Am Hubland, 97074 Wuerzburg (Germany)

    Dr. B. G. Kopek
    Hope College, Department of Biology
   35 E. 12th Street, Holland, MI 49423 (USA)

    Supporting information and ORCID(s) from the author(s) for this
    article are available on the WWW under http://dx.doi.org/10.1002/
    anie.201509649.
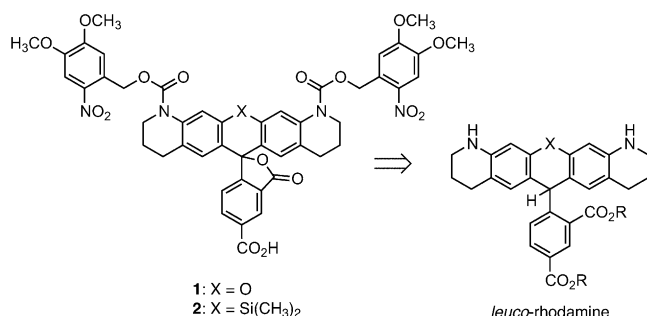
Scheme 1. Structural formula and retrosynthesis of photoactivatable ("caged") Rh_Q **1** and $SiRh_Q$ **2**.

envisioned creating a red-shifted isologue of caged Rh_Q in which the xanthene oxygen is replaced with a $(CH_3)_2Si$ moiety to yield caged Si-Q-rhodamine ($NVOC_2$-$SiRh_Q$, **2**; Scheme 1). The O-to-$(CH_3)_2Si$ modification elicits a desirable 100 nm bathochromic shift.[10] Such Si-rhodamines with an *o*-carboxyl group on the pendant phenyl ring have recently been shown to be excellent labels for microscopy,[11] but *N*-acyl or photoactivatable derivatives of these photostable Si-rhodamines have not been described.

We first prepared the unsubstituted $SiRh_Q$. As shown in Scheme 2, our synthesis starts with known 1-benzyl-7-bromo-
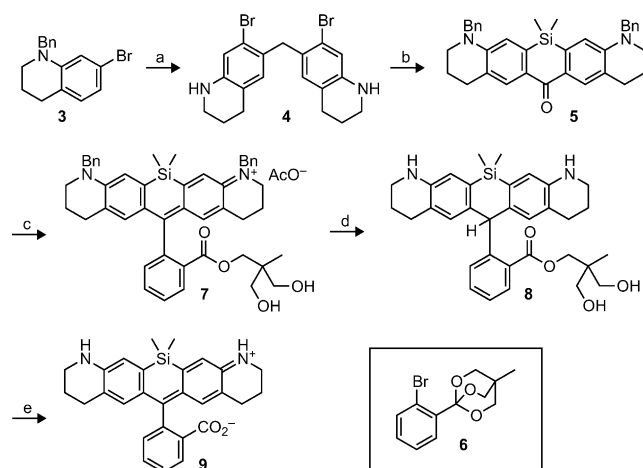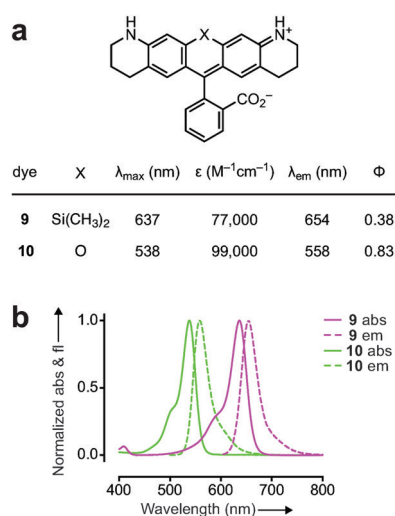

Scheme 2. Synthesis of $SiRh_Q$ (**9**). a) H_2CO, AcOH, 60°C, 77%. b) i. *sec*-BuLi, THF, −78°C, $(CH_3)_2SiCl_2$. ii. $KMnO_4$, acetone, −15°C, 37%, (two steps). c) *t*BuLi, **6**, THF, −78°C, 1 N HCl, 96%. d) NH_4HCO_2, Pd/C, CH_3OH/Et_2O, 50°C. e) i. LiOH, THF/H_2O, 55°C. ii. *p*-chloranil, CH_2Cl_2/CH_3OH, 68% (three steps).

1,2,3,4-tetrahydroquinoline (**3**). The *N*-benzyl protecting group was chosen to allow simultaneous deprotection of the aniline nitrogen atoms and reduction of the dye, which is needed later to achieve efficient installation of the caging groups via the *leuco*-dye strategy.[8c] Condensation of **3** with formaldehyde gave bis(tetrahydroquinolinyl)methane **4**. Lithiation and reaction with $(CH_3)_2SiCl_2$ installed the desired silicon atom, and subsequent oxidation with $KMnO_4$ gave Si-anthrone **5**.[11a, 12] Previously reported strategies to install the *o*-carboxyphenyl ring were met with limited success (Scheme S1 in the Supporting Information). We therefore

tried the orthoester protecting group, which has not been used in rhodamine syntheses. Lithiation of OBO-protected benzoate **6** and addition to **5** afforded Si-rhodamine ester **7** after workup with HCl. Catalytic hydrogenation gave *leuco*-rhodamine **8** with concomitant removal of the *N*-benzyl groups. Saponification followed by oxidation of the rhodamine core using *p*-chloranil gave the desired $SiRh_Q$ (**9**) in 68% over three steps. Interestingly, reduction was necessary for facile removal of the OBO residual 2,2-bis(hydroxymethyl)propyl ester. Attempts to hydrolyze this ester prior to reduction required forcing conditions that resulted in substantial decomposition of the desired Si-rhodamine.

We then evaluated the spectral properties of Si-Q-rhodamine (**9**) in comparison to those of Rh_Q (**10**).[8c] Rhodamine **10** shows absorbance maximum (λ_{max}) and fluorescence emission maximum (λ_{em}) at 538 nm and 558 nm, respectively, an extinction coefficient (ε) of $9.9 \times 10^4 \, M^{-1} \, cm^{-1}$, and a quantum yield value (Φ) of 0.83 (Figure 1). The silicon-analogue **9**

dye	X	λ_{max} (nm)	ε ($M^{-1}cm^{-1}$)	λ_{em} (nm)	Φ
9	$Si(CH_3)_2$	637	77,000	654	0.38
10	O	538	99,000	558	0.83

Figure 1. a) Spectral properties for rhodamines **9** and **10**. b) Absorption (abs) and fluorescence emission (em) spectra for rhodamines **9** and **10**. All measurements were taken in aqueous buffer (10 mM HEPES, pH 7.3).

exhibited the expected red-shift with a $\lambda_{max} = 637$ nm and $\lambda_{em} = 654$ nm. Surprisingly, $SiRh_Q$ **9** also showed a relatively large extinction coefficient ($\varepsilon = 7.7 \times 10^4 \, M^{-1} \, cm^{-1}$); previously prepared silarhodamine dyes exhibit significantly smaller absorptivity in aqueous solution ($\varepsilon < 2.5 \times 10^4 \, M^{-1} \, cm^{-1}$). The quantum yield value ($\Phi = 0.38$) was comparable to other Si-rhodamine dyes.[11]

Based on this promising spectroscopic result, we expanded our synthetic route to prepare caged $SiRh_Q$ derivative **2**, which bears a carboxyl group as a handle for bioconjugation (Scheme 3). The Si-anthrone **5** was treated with the aryllithium species from di-orthoester **11** followed by acid workup. We found it most efficient to simply retain the OBO residual esters as the necessary carboxyl protecting groups; the hydroxyl groups were peralkylated with MOMCl to afford silarhodamine diester **12** from **5** in 82% yield over two steps. Catalytic hydrogenation of **12** removed the *N*-
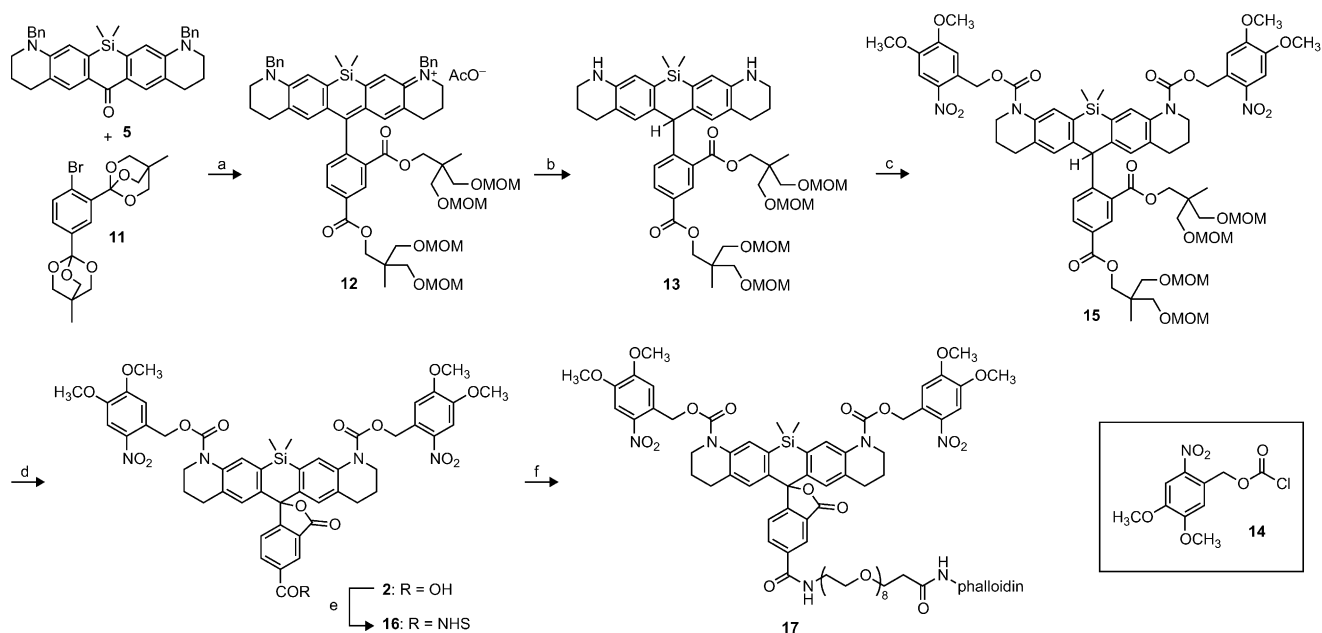
Scheme 3. Synthesis of 5-carboxy-NVOC$_2$-SiRh$_Q$ (**2**) and phalloidin conjugate **17**. a) i. *t*BuLi, THF, −78 °C, 1 N HCl. ii. MOMCl, DIEA, CH$_2$Cl$_2$, 82 % (two steps). b) NH$_4$HCO$_2$, Pd/C, CH$_3$OH/Et$_2$O, 50 °C. c) **14**, DIEA, CH$_2$Cl$_2$, 77 % (two steps). d) i. LiOH, THF/H$_2$O, 55 °C. ii. DDQ, CH$_2$Cl$_2$/H$_2$O, 86 % (two steps). e) TSTU, DIEA, DMF, 80 %. f) i. H$_2$N-PEG$_8$-CO$_2$H. ii. TSTU, DIEA, DMF. iii. phalloidin-NH$_2$, 50 % (three steps). DIEA = *N,N*-diisopropylethylamine; TSTU = *N,N,N′,N′*-tetramethyl-*O*-(*N*-succinimidyl)uronium tetrafluoroborate; DDQ = 2,3-dichloro-5,6-dicyano-*p*-benzoquinone.

benzyl protecting groups and reduced the dye, yielding *leuco*-rhodamine **13**. As before, the increased reactivity of the aniline nitrogen atoms in **13** allowed facile installation of the NVOC caging groups by acylation with **14** to give caged *leuco*-rhodamine **15**. Saponification of both ester groups using LiOH followed by oxidation with DDQ gave the desired caged SiRh$_Q$ **2** in 86 % yield. To use the free 5-carboxyl group as a conjugation handle, we prepared the *N*-hydroxysuccinimidyl ester **16**. From the activated ester, we synthesized a phalloidin conjugate of the dye (**17**) with a short 8-mer PEG linker ($\lambda_{max}/\lambda_{em}$ = 640 nm/655 nm after photoconversion, Figure S1).

We then tested the utility of the phalloidin conjugate **17** to image cellular F-actin on fixed COS-7 cells, comparing it to the commercially available Alexa Fluor 647-phalloidin conjugate (AF647-phalloidin), which has been used extensively in localization microscopy experiments.[13] Under optimal *d*STORM buffer conditions using a highly inclined and laminated optical sheet (HILO) setup,[14] the AF647-phalloidin gave high photon counts (median = 5547) and a localization precision of 5.7 nm (Figure S2). In the initial trial of conjugate **17** we imaged in non-degassed phosphate buffered saline (PBS). As with other NVOC caged dyes, there is sufficient absorption at 405 nm to allow activation with this common laser line.[8c,d] Using **17**, we observed similar results with higher photon counts per localization event (median = 9145) than AF647-phalloidin but lower theoretical localization precision (6.2 nm) owing to greater fluorescence background. This higher background in the PALM experiment could stem from the propensity of the molecule to adopt the zwitterionic form (shown in Figure 1). We then investigated whether we could improve the photon counts through the

addition of antibleaching agents. We discovered that the addition of Trolox[15] caused a dramatic performance improvement in oxygen-deprived buffer, giving an image of the cellular actin network (Figure 2a) with better localization precision (5.3 nm) than either previous experiment owing to substantially higher photon counts (median = 14944). This precision allowed high-resolution imaging of actin-rich structures, such as filopodia (Figure 2b,c) and smaller features (Figure S3).

Given its relatively long absorption maxima and excellent photophysics, we then tested the utility of caged SiRh$_Q$ with mEos2[4a] in multicolor localization microscopy. To evaluate the cross-talk between the two labels, we expressed a fusion protein containing mEos2 and a mitochondrial localization sequence and then stained F-actin with phalloidin conjugate **17**. Mitochondria do not contain actin but associate tightly with the cytoskeleton, providing an ideal test case. The cells were then imaged using iPALM under conditions optimized for mEos2.[2] Compound **17** and mEos2 exhibited sufficiently different activation cross-sections to allow successive imaging of the two colors. The actin was imaged first using 1 W cm^{-2} of 405 nm light to activate the SiRh$_Q$ and 640 nm to excite the uncaged fluorophore. This low level of activation light and long-wavelength excitation preserved over 90 % of the mEos2, which could be activated with higher intensity 405 nm light (10 W cm^{-1}) and excited with 561 nm light. The results are shown in Figure 3 with the mitochondrial mEos2 marker rendered in green and the SiRhQ probe shown in red. We observe excellent staining of both the mitochondria and the actin. Importantly the expanded images in both the *x,y* and *x,z* planes show no cross-talk between the two dyes. This experiment is the first example of multicolor localization
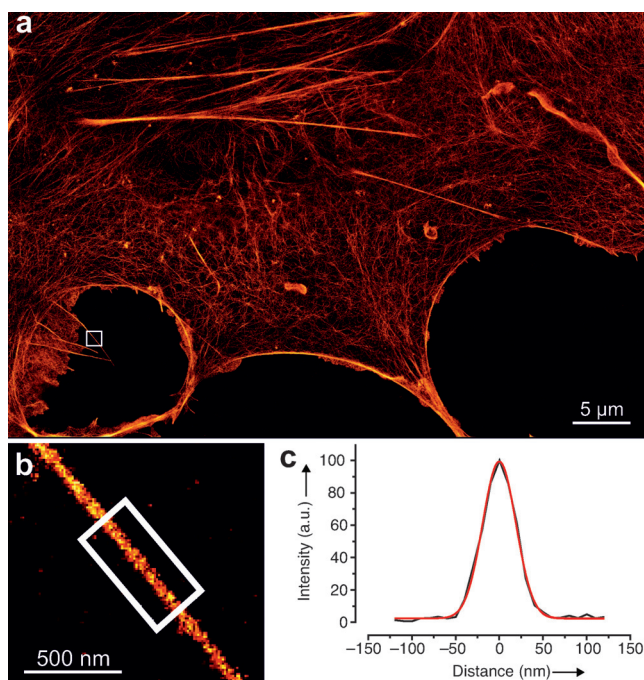
Figure 2. a) Localization microscopy image (HILO) of COS-7 cell stained with phalloidin conjugate **17**; scale bar: 5 µm. b) Expanded image of boxed region in (a) showing a protruding filopodial structure. c) Line-scan intensity across filopodial structure in (b; black) and Gaussian fit (red). Full width at half maximum (FWHM) = 45 nm.
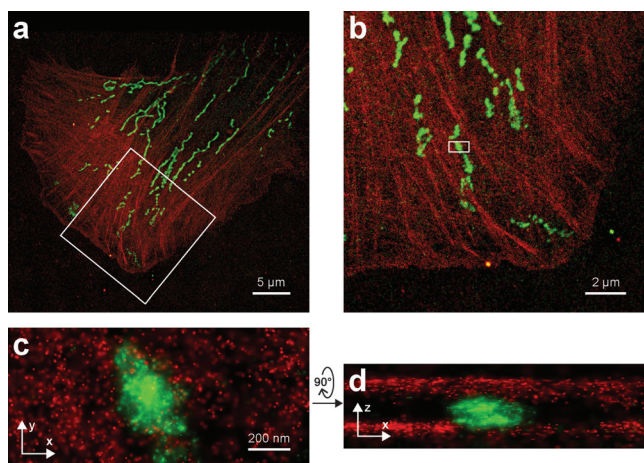
Figure 3. a) Two color iPALM image of a fixed U2OS cell labeled with phalloidin conjugate **17** (actin, red) and mEos2 (mitochondria, green). b) Enlarged image of boxed area in (a). c) *x,y* projection of boxed area in (b). d) *x,z* projection of boxed area in (b).

microscopy using a caged dye and a photoconvertible fluorescent protein, validating SiRh$_Q$ as a new label for multicolor PALM imaging.

In summary, we describe the design and synthesis of the first photoactivatable Si-rhodamine and demonstrate its utility in localization microscopy. The probe exhibits higher photon counts than the standard Alexa Fluor 647 label and circumvents the use of reducing buffers to elicit photoswitching, making it relatively simple to implement. These mild imaging conditions and the red-shifted spectra also enable accurate, multicolor, 3D super-resolution imaging with a photoconvertible fluorescent protein mEos2. The phalloidin conjugate **17** should enable careful interrogation of protein interactions with the cytoskeleton. We have now described flexible and efficient chemical routes towards different caged rhodamine dyes with absorption maxima spanning 490–640 nm.[8c,d] With this chemistry in hand, the remaining challenge lies in improving the biocompatibility of these caged dyes by increasing their water solubility and incorporating these molecules into known labeling strategies to tag cellular components. This effort will produce a palette of caged fluorophores useful for the preparation of reagents including antibody conjugates, tagged oligonucleotides, and ligands for self-labeling tags. Such probes will be valuable tools for multicolor localization imaging and other single-molecule microscopy experiments. Finally, the long-wavelength absorption and unexpected large extinction coefficient of SiRh$_Q$ make it an exciting scaffold for other fluorogenic molecules, such as enzyme substrates and reaction-based sensors.[16]

How to cite: *Angew. Chem. Int. Ed.* **2016**, *55*, 1723–1727
Angew. Chem. **2016**, *128*, 1755–1759

[1] a) E. Betzig, G. H. Patterson, R. Sougrat, O. W. Lindwasser, S. Olenych, J. S. Bonifacino, M. W. Davidson, J. Lippincott-Schwartz, H. F. Hess, *Science* **2006**, *313*, 1642–1645; b) S. T. Hess, T. P. K. Girirajan, M. D. Mason, *Biophys. J.* **2006**, *91*, 4258–4272; c) M. J. Rust, M. Bates, X. Zhuang, *Nat. Methods* **2006**, *3*, 793–796; d) M. Heilemann, S. van de Linde, M. Schüttpelz, R. Kasper, B. Seefeldt, A. Mukherjee, P. Tinnefeld, M. Sauer, *Angew. Chem. Int. Ed.* **2008**, *47*, 6172–6176; *Angew. Chem.* **2008**, *120*, 6266–6271.

[2] G. Shtengel, J. A. Galbraith, C. G. Galbraith, J. Lippincott-Schwartz, J. M. Gillette, S. Manley, R. Sougrat, C. M. Waterman, P. Kanchanawong, M. W. Davidson, H. F. Hess, *Proc. Natl. Acad. Sci. USA* **2009**, *106*, 3125–3130.

[3] a) M. F. Juette, T. J. Gould, M. D. Lessard, M. J. Mlodzianoski, B. S. Nagpure, B. T. Bennett, S. T. Hess, J. Bewersdorf, *Nat. Methods* **2008**, *5*, 527–529; b) B. Huang, W. Wang, M. Bates, X. Zhuang, *Science* **2008**, *319*, 810–813; c) M. K. Lee, P. Rai, J. Williams, R. J. Twieg, W. E. Moerner, *J. Am. Chem. Soc.* **2014**, *136*, 14003–14006.

[4] a) S. A. McKinney, C. S. Murphy, K. L. Hazelwood, M. W. Davidson, L. L. Looger, *Nat. Methods* **2009**, *6*, 131–133; b) B. Moeyaert, N. Nguyen Bich, E. De Zitter, S. Rocha, K. Clays, H. Mizuno, L. Van Meervelt, J. Hofkens, P. Dedecker, *ACS Nano* **2014**, *8*, 1664–1673.

[5] a) M. Heilemann, E. Margeat, R. Kasper, M. Sauer, P. Tinnefeld, *J. Am. Chem. Soc.* **2005**, *127*, 3801–3806; b) G. T. Dempsey, J. C. Vaughan, K. H. Chen, M. Bates, X. Zhuang, *Nat. Methods* **2011**, *8*, 1027–1036.

[6] a) S. van de Linde, I. Krstić, T. Prisner, S. Doose, M. Heilemann, M. Sauer, *Photochem. Photobiol. Sci.* **2010**, *10*, 499–506; b) J. C. Vaughan, S. Jia, X. Zhuang, *Nat. Methods* **2012**, *9*, 1181–1184; c) L. Carlini, A. Benke, L. Reymond, G. Lukinavičius, S. Manley, *ChemPhysChem* **2014**, *15*, 750–755; d) M. Lehmann, B. Gottschalk, D. Puchkov, P. Schmieder, S. Schwagerus, C. P. R. Hackenberger, V. Haucke, J. Schmoranzer, *Angew. Chem. Int. Ed.* **2015**, *54*, 13230–13235; *Angew. Chem.* **2015**, *127*, 13428–13433.

[7] G. T. Dempsey, M. Bates, W. E. Kowtoniuk, D. R. Liu, R. Y. Tsien, X. Zhuang, *J. Am. Chem. Soc.* **2009**, *131*, 18192–18193.

[8] a) J. Fölling, V. Belov, R. Kunetsky, R. Medda, A. Schönle, A. Egner, C. Eggeling, M. Bossi, S. W. Hell, *Angew. Chem. Int. Ed.* **2007**, *46*, 6266–6270; *Angew. Chem.* **2007**, *119*, 6382–6386; b) H. D. Lee, S. J. Lord, S. Iwanaga, K. Zhan, H. Xie, J. C. Williams, H. Wang, G. R. Bowman, E. D. Goley, L. Shapiro, R. J. Twieg, J. Rao, W. E. Moerner, *J. Am. Chem. Soc.* **2010**, *132*, 1642–1645; c) L. M. Wysocki, J. B. Grimm, A. N. Tkachuk, T. A. Brown, E. Betzig, L. D. Lavis, *Angew. Chem. Int. Ed.* **2011**, *50*, 11206–11209; *Angew. Chem.* **2011**, *123*, 11402–11405; d) J. B. Grimm, A. J. Sung, W. R. Legant, P. Hulamm, S. M. Matlosz, E. Betzig, L. D. Lavis, *ACS Chem. Biol.* **2013**, *8*, 1303–1310; e) V. N. Belov, G. Y. Mitronova, M. L. Bossi, V. P. Boyarskiy, E.

Hebisch, C. Geisler, K. Kolmakov, C. A. Wurm, K. I. Willig, S. W. Hell, *Chem. Eur. J.* **2014**, *20*, 13162–13173.

[9] K. Kolmakov, C. Wurm, M. V. Sednev, M. L. Bossi, V. N. Belov, S. W. Hell, *Photochem. Photobiol. Sci.* **2012**, *11*, 522–532.

[10] Y. Koide, Y. Urano, K. Hanaoka, T. Terai, T. Nagano, *ACS Chem. Biol.* **2011**, *6*, 600–608.

[11] a) G. Lukinavičius, K. Umezawa, N. Olivier, A. Honigmann, G. Yang, T. Plass, V. Mueller, L. Reymond, I. R. Corrêa, Jr., Z. G. Luo, C. Schultz, E. A. Lemke, P. Heppenstall, C. Eggeling, S. Manley, K. Johnsson, *Nat. Chem.* **2013**, *5*, 132–139; b) J. B. Grimm, B. P. English, J. Chen, J. P. Slaughter, Z. Zhang, A. Revyakin, R. Patel, J. J. Macklin, D. Normanno, R. H. Singer, T. Lionnet, L. D. Lavis, *Nat. Methods* **2015**, *12*, 244–250.

[12] T. Egawa, Y. Koide, K. Hanaoka, T. Komatsu, T. Terai, T. Nagano, *Chem. Commun.* **2011**, *47*, 4162–4164.

[13] K. Xu, G. Zhong, X. Zhuang, *Science* **2013**, *339*, 452–456.

[14] M. Tokunaga, N. Imamoto, K. Sakata-Sogawa, *Nat. Methods* **2008**, *5*, 159–161.

[15] T. Ha, P. Tinnefeld, *Annu. Rev. Phys. Chem.* **2012**, *63*, 595–617.

[16] a) J. Chan, S. C. Dodani, C. J. Chang, *Nat. Chem.* **2012**, *4*, 973–984; b) J. B. Grimm, L. M. Heckman, L. D. Lavis, *Prog. Mol. Biol. Transl. Sci.* **2013**, *113*, 1–34.